RESEARCH METHODS VOLCANICA

Submitted: 2022-08-30 | Accepted: 2023-02-25 | Published: 2023-04-11

Drone-deployed sensors: a tool for multiparametric near-vent measurements of volcanic explosions

Markus Schmid*[α], Ulrich Kueppers[α], Johannes Huber[β], and Donald B. Dingwell[α]
[α] Department of Earth and Environmental Sciences, Ludwig-Maximilians-Universität München, 80333 Munich, Germany.
[β] Hubersoft, Öhmdwiesenweg 10, 78476 Allensbach, Germany.

Abstract

Observations and measurements on active volcanoes are commonly conducted at a distance considered safe from the inherent dangers linked to volcanic explosions. This reduction in proximity adds a degree of uncertainty to the interpretation of monitoring data due to enhanced signal path effects. Here, we describe custom-built, drone-deployable sensor platforms designed to acquire data at high proximity to volcanic vents. They are equipped with an environmental sensor capable of measuring temperature, relative humidity and barometric pressure, a microphone (6 Hz–20 kHz) to reconstruct the acoustic pressure, and an electrical resonant circuit to detect electrical signals in the 500 kHz frequency band. Communication and data transfer is achieved through a radio link between the sensor platform and the base station. Our sensor platforms may be employed in the collection of data of near-vent characteristics of volcanic explosions, observations that are essential for quantifying and understanding the driving forces underlying volcanic explosions.

Keywords: UAV; Explosive volcanism; Acoustic; Volcanic lightning; Infrasound; Sensors.

1 Introduction

Volcanic eruptions are dynamic and complex events that link Earth's interior to its surface. Human global population growth continues to result in increasing impingement of human settlement closer to active volcanic areas with a concomitant increase in society's exposure to volcanic risk [Freire et al. 2019]. Next to a plethora of solids, liquids, and gases, volcanoes emit acoustic, seismic, and electrical signals in eruptive phases. Technological advances and increased computational power now enable the acquisition of an unprecedented level of detail in the observation, modelling, and analysis of volcanic eruptions such as the use of uncrewed aerial vehicles (UAVs) [e.g. James et al. 2020, and references therein] and high-resolution satellite imagery [e.g. Carn et al. 2016, and references therein]. Direct observations of volcanic explosions are limited to the processes above the vent. To date, reconstruction of source parameters largely relies on ground-based observations which are most accurate when measured close to the vent. Yet, instruments of monitoring networks that typically require stable installation on the ground, maintenance, and/or data downloading can only be practically installed at a safe distance, inevitably excluding the direct surroundings of the vents of explosive eruptions. Here, we propose a solution to the dilemma of instrument accessibility to vents in the form of UAV-deployable systems to measure temperature, relative humidity, barometric pressure, and acoustic and electrical signals.

A big challenge in volcano monitoring is linking observable surface signals to sub-surface conditions. With the aid of scaled laboratory experiments as well as numerical and theoretical models, the influence of reservoir volume, pressure and vent geometry have been established [e.g. Ogden et al. 2008; Koyaguchi et al. 2010; Schmid et al. 2020; Cigala et al. 2021; Schmid et al. 2022]. Thus, a basis for the interpretation of surface signals has been generated and reliable measurements at the vent have become the remaining prerequisite for an estimation of source parameters. In this context we need to discriminate between the pressure at the source, i.e. the driving pressure of the volcanic explosion at fragmentation level, and the pressure (waves) that are emitted into the atmosphere at the vent. Here, we demonstrate the feasibility of measuring the pressure of the explosion close to the vent to retrieve high-quality data that can eventually be used to reconstruct the source parameters. Pressure waves emitted by volcanic eruptions are typically measured with microphones and micro-barometers.

1.1 Volcano acoustics

The analysis of acoustic emissions of volcanic eruptions has developed into a mature field [Fee and Matoza 2013]. To determine the pressure of volcanic explosions, infrasound is especially useful as it reveals information about the physical motion (i.e. the explosion) at the vent [Johnson 2003]. Volcanic infrasound (<20 Hz) is transmitted over long distances and the related recordings can be divided as local (<15 km), regional (15–250 km) and global (>250 km). For a comprehensive review of volcanic infrasound refer to Johnson and Ripepe [2011], Fee and Matoza [2013], Garcés et al. [2013], De Angelis et al. [2019], and Matoza et al. [2019]. Regional and global infrasound provide a possibility to monitor remote volcanoes where no local monitoring instrumentation is installed. Local recordings of infrasound can be used to estimate eruption parameters like gas exit velocity [e.g. Woulff and McGetchin 1976; Matoza et al. 2013; McKee et al. 2017], excess pressure [e.g. Ripepe and Marchetti 2002; Johnson 2003; 2004], erupted volume and mass [e.g. Johnson and Miller 2014; Kim et al. 2015; Delle Donne et al. 2016; Fee et al. 2017], geometry of the plumbing system, vents, and craters [Garcés 2000; Johnson

* markus.schmid@min.uni-muenchen.de

Editor: T. Pering | Typesetter: J. I. Farquharson

et al. 2018; Muramatsu et al. 2018; Watson et al. 2019; Taddeucci et al. 2021], and plume height [Caplan-Auerbach et al. 2010; Ripepe et al. 2013; Lamb et al. 2015].

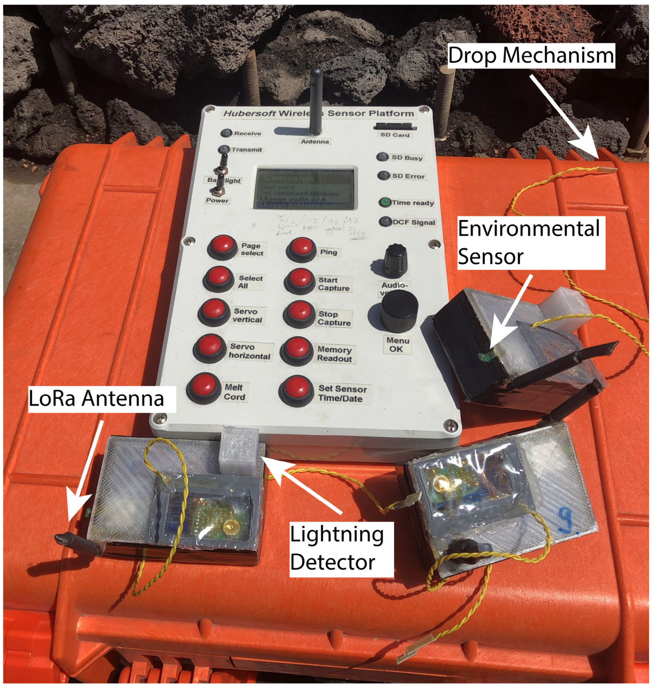

Figure 1: Base station and three sensors including drop mechanism ready for deployment. The base station is equipped with a primary antenna for the communication with the sensors and a secondary internal antenna to receive the DCF77 time signal. Downloaded data is stored on exchangeable SD card. Sensors are equipped with a primary monopole antenna for the LoRa communication and a secondary antenna for the lightning detection resonant circuit. The environmental BME 280 sensor is located on the outside of the housing, while the microphone is inside the housing protected by a membrane still allowing the detection of acoustic signals. The yellow chord is the drop-off mechanism. A bright LED is located below the membrane for a visual check of signal reception.

Early studies have assumed that infrasound signals that were recorded 'near the vent' (<5 km) are representative of the signals at the source because of the homogeneity of the atmosphere without structures affecting acoustic wave propagation. However, there is growing evidence that non-linear near-vent propagation [Maher et al. 2020], local topography [e.g. Lacanna and Ripepe 2013; Ishii et al. 2020; Lacanna and Ripepe 2020] and atmospheric conditions (wind, temperature, and density contrasts due to the presence of ash) [e.g. Johnson 2003; Lacanna and Ripepe 2013] substantially affect the signals recorded even at distances of few hundred metres.

Studies using acoustic signals in the audible frequency band are less frequent [e.g. Goto et al. 2014; Taddeucci et al. 2014; Lorenz et al. 2016] compared to studies using infrasound, partly because audible sound is more affected by attenuation. In a study using wideband acoustic observations at Stromboli volcano, Italy, Goto et al. [2014] found that gas-dominated explosions could only be detected in the audible frequency spectrum. For explosions that emit both infrasound and audible acoustic signals, it was proposed that the initial infrasound is generated by the doming of the lava surface of a large bubble just before its rupture [Ripepe et al. 2001; Kobayashi et al. 2010; Vidal et al. 2010; Goto et al. 2014]. Vergniolle et al. [1996] proposed that the audible sound of explosions at Stromboli may be generated by collisions of fragmented ejecta with the ground or conduit while Goto et al. [2014] suggested eddies within the expanding jet or highly 'pressurized gas sprays' after the initial bubble burst as origin of the audible sound. Peña Fernández et al. [2020] identified up to five different source components for the origin of the audible sound of rapid decompression experiments in an anechoic chamber. In particular, volcanic explosions with high-velocity jets of gas (with or without a solid and liquid component) are known to radiate acoustic signals in the audible frequency range [Tam 1995].

To date, the pressure of an explosion has either been denoted as 'corrected for the distance to the source' or as 'pressure at the recording distance'. There is a wide agreement that atmospheric (e.g. wind, temperature, inhomogeneities) and boundary conditions (e.g. topography, vent geometry) must be taken into consideration when using acoustic signals to infer source conditions. Still, in the absence of vent-proximal data, our knowledge about how to correct acoustic data recorded 'away from volcanic vents' for all these factors remains incomplete.

1.2 Volcanic lightning

Volcanic eruptions frequently produce lightning over a wide range of explosive styles and magnitudes [Cimarelli and Genareau 2021]. However, there seems to be an observational bias towards lightning observations during large explosions with a majority of reports for eruptions with a Volcanic Explosivity Index (VEI) > 2 [McNutt and Williams 2010]. Volcanic lightning can be used as a monitoring tool to confirm volcanic eruptions in remote areas and where visual confirmation is not possible [Behnke and McNutt 2014]. Lightning processes emit electromagnetic signals with a wide frequency range (1 Hz to near 300 MHz) [Rakov 2013]. The relationship between volcanic lightning and eruption parameters (e.g. plume height, mass eruption rate, and grain size distributions) has been investigated [e.g. Bennett et al. 2010; Gaudin and Cimarelli 2019; Hargie et al. 2019; Vossen et al. 2021; 2022]. However, the electrical properties of eruptions on the lower end of the VEI have been largely overlooked [Cimarelli and Genareau 2021].

To fill these knowledge gaps, here we have developed lightweight sensor platforms for deployment by UAV within a few metres of the volcanic vent in order to measure temperature, humidity, barometric pressure, the acoustic pressure at the vent exit, and to detect low magnitude volcanic lightning discharges.

2 Methodology

2.1 Sensor platforms

Deployment of sensor platforms (SPs) close to active volcanic vents inevitably includes some potential exposure to eruptive activity. Accordingly, the development of the SPs here has been focused on minimizing material costs and weight to allow for deployment by commercially available UAVs (*DJI Phantom 4Pro+*). Including batteries and the drop mechanism, each SP weighs less than 150 g and material costs are less than 50 €. The SPs contain different sensors to measure barometric pressure, temperature, humidity, acoustic signals, and electrical discharges. The setup described here is a combination of one base station and several UAV-deployable SPs (Figure 1). Each SP is controlled by a microcontroller and comprised of several sensors:

- Absolute barometric pressure, temperature, and humidity are measured with a BOSCH *BME 280* environmental sensor with a sample frequency of 20 Hz.

- Acoustic signals are recorded by a microphone (InvenSense *ICS-40300*) with a frequency range of 6 Hz to 20 kHz at a sample rate of 32 kHz. The sensitivity of the microphone is −45 dBV. The recorded acoustic data is averaged over groups of 32 samples each, reducing the effective sample rate to 1000 Hz, acting as a low-pass filter with a cut-off frequency of 500 Hz. We also calculate the maximum amplitude for each group containing 32 samples.

- Monitoring of electrical discharges is accomplished through an amplitude modulation (AM) radio amplifier and an antenna in an electrical resonant circuit with a resonance frequency of 500 kHz. If a lightning event occurs, the resonant circuit oscillates. The number of oscillations is summed over a window of 10 ms and recorded at 100 Hz ('lightning sum', see Figure 3).

Temperature and humidity data are used to calibrate the barometric pressure and to monitor sensor health. The environmental sensor shows the pressure variation of the atmosphere. The pressure of the volcanic explosion is measured from the amplitude of the acoustic signals. The first generation of this sensor platform revealed shortcomings in the interpretability of acoustic data (raw data information was lost during on-board processing) that are being tackled in ongoing sensor platform development.

Each SP is powered by three AA batteries which last for 1.4 years in standby mode, and allow 60 hours of measurements and 10–12 hours of data transmission with the highest transmission power (40 hours with lowest). In recording mode, all data is written to a ring buffer (128 kB) with a capacity of 38 s of data. When the ring buffer is full, the oldest data is continuously overwritten by newer data, meaning that at any given time the last 38 s of data are stored when data recording is stopped. The data can be downloaded to the base station where it is saved on a SD card (500 metres away in case of Stromboli volcano, Italy, where our system was successfully tested). Data transfer and communication between base station and individual SPs is achieved over LoRa (Long Range) radio communication in the license-free 433.05–434.79 MHz frequency band using a coiled monopole antenna. The advantage of using LoRa is its capability of long-range transmission at low power consumption. The implemented communication protocol was designed to enable individual as well as simultaneous communication with multiple active SPs while eliminating the risk of data loss and corruption during transmission.

Arrays of three or more SPs are ideal to characterize the distance-dependent signals of individual volcanic eruptions. To build such arrays, the drop mechanism of individual SPs was attached to a nylon line (0.35 mm) suspended below a UAV and flown to the desired location. For deployment, an electrical signal melts the connection to the line. The sensors are enclosed in a custom-built, 3D-printed housing that provides protection for the electrical components against ash fall, adverse weather conditions, and corrosive gases. All SPs are time-synchronised through the DCF77 (longwave time signal) time code transmitter that can be received by the base station and distributed to all sensors.

2.2 Field campaigns

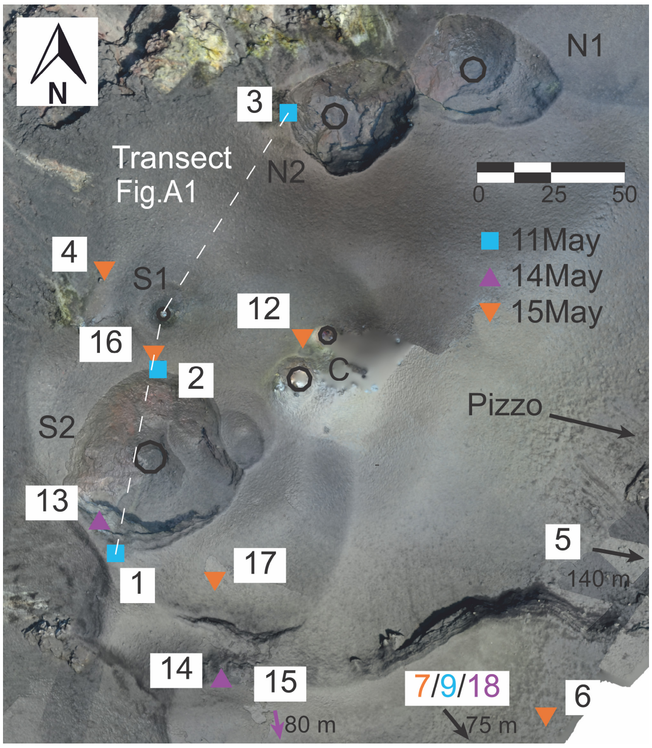

Figure 2: Crater Terrace of Stromboli volcano, Italy, as in May 2019 [Schmid et al. 2021]. Sensor locations were located in a georeferenced orthomosaic via georeferenced images taken during the placement of the senor. The colour of symbols indicates on which day the sensors were operational. The dashed white line marks a transect that can be seen in Figure A1. Refer to Table 1 for all vent to sensor distances.

The feasibility of near-vent sensor deployment was tested during two field campaigns to Stromboli volcano, Aeolian Islands, Italy, in September 2018 (first generation) and May 2019 (second generation). During the 2018 campaign (9, 10, 12 September) we tested different deployment strategies including dropping the SPs from up to several tens of metres height which was survived by all SPs. For the 2019 campaign we improved the housing, restructured the use of the ring buffer, and added the sensor for electrical discharges. In May 2019 the second generation of SPs was used during three days of data acquisition (11, 14, and 15 May). We deployed 13 SPs in total. Due to volcanic activity (SPs being destroyed by bombs) and substantial rainfall, SP arrays had to be created on each of the three days. Overall, we recorded 47 events (i.e. sin-

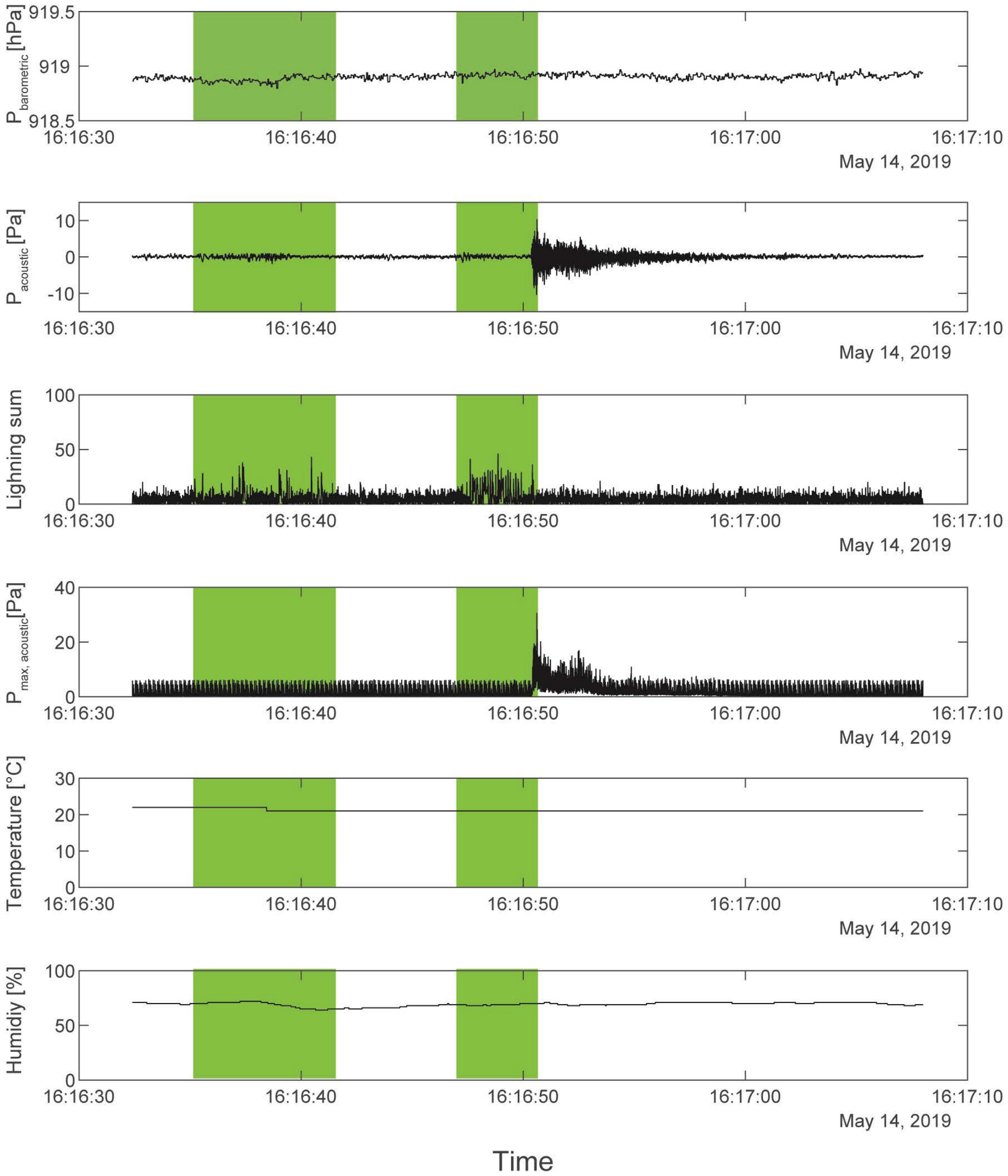

Figure 3: Dataset recorded by sensor 14 during an explosive event on 14 May 2019 at 16:16 UTC at a distance of 136 m from the vent. This plot shows the barometric pressure, acoustic pressure, lightning sum, maximum acoustic pressure, temperature and relative humidity. Areas with green background indicate periods with electrical activity. Refer to Figure 4A and B for the acoustic signals of all operational SPs.

gle explosive eruptions) with up to four SPs simultaneously. In May 2019, the crater terrace was divided into three active vent areas: north-east (N), south-west (S) and central (C) (see Figure 2 and Civico et al. [2021]; Pering et al. [2020]; Schmid et al. [2021]). In the N area, two vents (N1 and N2) were active, showing predominantly ash-rich explosions, at times accompanied by bombs. In the S area, two vents (S1 and S2) were active. While the S2 vent exhibited ash-rich explosions with bombs, the activity of S1 was characterised by gas-rich jets up to 40 s duration. These jets had increased in duration and intensity since 2018 [Taddeucci et al. 2021] and were the target of this study. Following an explosion on 14 May 2019 in the morning, its morphology was changed, leading to significantly changed eruption characteristics. The duration of the jets was shorter and the ash content was significantly higher. The two central vents were passively degassing with visible incandescence and occasional gas puffing. For a comprehensive description of the crater terrace morphology and the activity refer to Schmid et al. [2021].

During the 2019 campaign we worked as a three-person team for the deployment of the SPs. One person piloted the UAV, the second person operated the SP base station, monitoring signal strength and triggering the drop mechanism. The third person attached the SPs to the UAV and monitored the volcanic activity during flight. All flights were conducted manually without preprogrammed flight paths in order to be able to react quickly to volcanic explosions and prevent damage to or loss of the UAV. We took off with the UAV directly after an explosion to use the time in between explosions for the near-vent deployments.

The SPs were suspended 2.5–3 m below the UAV, a *DJI Phantom 4 Pro*. Once a SPs was placed on the ground at the planned location, the connection was released, the SP was put in recording mode, and the UAV returned to the take-off location to be equipped with the next SP. The exact position of the deployed SPs was reconstructed via the drone's GPS by utilising geo-tagged images and video footage of the drop location to locate the SPs on a photogrammetric model of the crater terrace. The SP-to-vent distances were corrected for their elevation difference and were between 15 and 354 m (see Table 1 and Figure 2). After an explosion considered worthy of saving the data, the recording on all active SPs was stopped and the data were downloaded to the base station. This prevents loss of data in case a SP was destroyed by subsequent explosions. The temperature and humidity data can be used as a real time monitoring tool for the presence of gas or bomb fallout close to a SP and therefore help to judge sensor health remotely.

Table 1: Distance between sensor platforms and all the vents as of May 2019. The listed distances represent the line-of-sight accounting for horizontal and vertical differences. Distances were obtained by locating the sensor positions in a photogrammetric model of Stromboli's crater terrace.

SP	Distance to vent [m]			
#	S1	S2	N1	N2
1	91	51	239	191
2	18	42	175	122
3	87	145	87	41
5	321	328	303	320
6	319	303	354	349
7	280	253	327	320
9	280	253	327	320
12	51	76	120	90
13	80	42	228	185
14	136	104	264	230
15	230	197	330	304
16	15	45	162	116
17	98	69	222	179
18	280	253	327	320

3 Results

We developed, tested, and deployed this novel piece of instrumentation to collect multiparametric data as close as possible to volcanic vents. In May 2019 the second generation of SPs was successfully used to measure barometric pressure, temperature, humidity, acoustic signals, and electrical discharges at distances considerably closer than accomplished before. The deployment via UAV worked flawlessly and we did not encounter any in-flight problems due to the volcanic activity. Although the *DJI Phantom 4 Pro* has no capability to transport payloads according to the manufacturer's specifications we found that 0.5 kg could be transported without any issues. Where possible we approached the near-vent locations from an upwind direction to avoid contact with emitted ash or gas plumes from open vents or fumaroles. Because of the simple design of the drop mechanism, we did not encounter any issues with releasing the sensors at their designated location as long as there was radio connection between SP and base station.

Overall, we recorded 47 events with up to four SPs simultaneously. Out of 13 SPs deployed, a maximum of 4 were operational at any given time. First of all, the deployment works on a one-by-one basis and it was not a priority to deploy the sensors quickly, but rather to test different deployment locations and strategies, to make sure that the radio link was stable and avoid damage to the UAV. Secondly, there were two days of bad weather between the first and second day of deployment and despite weatherproofing the sensors with a sealed 3D-printed housing the substantial rainfall strained the sensor's water resistance. Furthermore, we also deployed sensors in high-risk locations to test the effect of ash and bomb fall in the vicinity or on the sensors, leading to destruction of sensors and reducing the number of operational sensors. Ash fall did not have an effect on the sensor recording or transmission capabilities, unless the sensor's antenna was buried by substantial amounts of ash. In contrast, bomb impacts on and near the sensor led to quickly rising temperatures and eventually loss of connection to the sensor. The lifespan of sensors deployed on thermal anomalies (ca. 60–80 °C), (likely resulting from diffuse degassing), was also shorter compared to sensors without this additional thermal and chemical stress. Out of these 47 events, 37 yielded plausible data, here we present representative data of three events to demonstrate the potential of a near-vent deployments of these SPs.

On 14 May 2019 at 16:16:51 UTC, we recorded an explosion of the S1 vent with three SPs (#14 at 136 m, #15 at 230 m, and #18 at 280 m distance, respectively) with a peak pressure of 10.2 Pa measured by SP14. The maximum pressure measured at the sensors located further away, were 6.3 Pa (#15) and 4.8 Pa (#18). This dataset contains two periods with electrical activity that are only visible in the data of SP 14 (Figure 3). In the datasets of the two other SPs located further away from the vent areas the signal-to-noise ratio is too low to identify these signals. The discharge signals did not concur with the main explosion of the S1 vent but coincided with smaller acoustic events beforehand, most likely from a different vent. The onsets of the two smaller acoustic events matched precisely the onset of the electrical signals which continued for 1.5-2.2 s longer than the acoustic events. These acoustic events were identified in all three datasets of the deployed SPs (Figure 4A and B) with peak pressures considerably lower than during the explosion at the S1 vent (1.2 Pa, #14; 0.7 Pa, #15; 0.6 Pa, #18; Figure 4B). Unfortunately, the visibility during most of the campaign was limited and we lack visual observations of the nature of the acoustic events. In the acoustic waveforms different eruptive styles, such as explosions, gas jetting, and gas puffing (Figure 4) could be identified. On 15 May 2019 at 12:49:27 we recorded an event at the S1 vent with 3 SPs (#12 at 51 m, #5 at 321 m, and #6 319 m distance). The periodic puffing activity at the C vents was only detected in the data of SP12 located directly adjacent to the vents with a maximum pressure of around 4 Pa. The ash-rich jetting event at S1 was recorded by all active sensors with peak pressures of 10.0 Pa (#12), 9.4 Pa (#6), and 8.0 (#5). The jetting was considerably shorter and did show more variation in amplitude (Figure 4C) than before the modification of the vent geometry (early morning of 14 May 2019) when long and powerful jetting activity dominated (Figure 4D). We show data for one of these long jetting events that occurred on 11 May 2019 at 12:59:08 UTC. The peak pressure was 18.3 Pa for the closest SP (#2 at 18 m), 17.9 (#1 at 90 m), 5.0 Pa, and 1.6 Pa (#3 at 87 m and #9 at 280 m). Despite the small difference in their distance to the vent (3 m), SP 1 and 3 show a striking difference in their maximum amplitude (Figure 4) which can only be explained by the topography around the SPs (Figure A1).

Throughout all datasets we could see a difference in arrival times as a consequence of distances from the acoustic source. However, the measured arrival times did not match the expected arrivals when assuming homogeneous propagation of the acoustic waves. We illustrate this for a dataset of a jetting event on 15 May 2019 at 12:14 UTC at the S1 vent recorded with four SPs at distances of 15 m (#16), 51 m (#12), 321 m (#5), and 319 m (#6), respectively (see Figure 2 and 5). The onset of the explosion is delayed by 145 ms in the data of SP 12 compared to the closest SP (#16). The signal arrived 927 ms (#5) and 872 ms (#6) after its arrival at SP 16. Based on arrival times and the line-of-sight distances between SPs we calculated the propagation velocity to the different sensors (250 m s^{-1}, #12; 330 m s^{-1}, #5; 348 m s^{-1}, #6). The amplitudes of the maximum positive pressure peak were 22.5 Pa (#16), 15.2 Pa (#12), 10.4 Pa (#5), and 13.0 Pa (#6), revealing a non-linear pressure decay.

4 Discussion

We demonstrate the feasibility of deploying sensors with UAVs in the proximity of active volcanic vents. This, together with routine monitoring data, will augment our quantitative understanding of the boundary conditions of these explosions. We identified the associated opportunities and challenges of such near-vent measurements and continue developing the sensor platforms.

The dataset of 14 May 2019, 16:16 UTC (see Figure 3) was the only dataset that did show distinctive signals of electrical discharges. However, these signals did not coincide with the acoustic signal of the main explosion of S1 but with smaller acoustic events before. The onset of the electrical signal and the acoustic event coincide, but the electrical signals continue until after the acoustic event is over. We propose that these signals were linked to (inaudible) ash venting or ash-rich puffing from a different vent prior to the explosion at the S1 vent. In this case, electrical signals can be generated in the rising ash plume even after the acoustic event (explosion) has ceased [Vossen et al. 2022]. The acoustic events could be identified in all datasets, confirming the events (see Figure 4A and B). Unfortunately, visibility was limited due to cloud coverage and we lack observations to verify the source of the acoustic events. Since our observations were focused on the gas-rich jetting events at S1, events with the potential for electrical discharges at other vents may be underrepresented in the present dataset. Nevertheless, it proves the sensitivity of our sensors and the generation of electric signals. The sensors placed further away did record the acoustic events linked to the electrical signals but could not detect electrical discharges. Since the electric field decreases proportional to the distance cubed from the discharge location, it seems that magnitude of the discharges was too small to be picked up by the more distant sensors. This supports the findings of Vossen et al. [2022] that electrical discharges can occur also during low VEI activity, as it is common during normal Strombolian explosions and further highlights the necessity of near-vent instrumentation.

The dataset of the jet recorded on 11 May 2019 at 12:58:08 UTC shows a distinctive difference in the signals measured by SP3 and SP1. The acoustic signal arrived 13 ms seconds earlier at SP3 (87 m) than at SP1 (90 m). However, both SPs show a distinctive difference in the maximum amplitude of the acoustic pressure (17.9 Pa, #1 and 5 Pa, #3) as a result of the topography of the surrounding of the SPs. While SP1 had a direct line-of-sight placed 10 m above the S1 vent, direct line-of-sight was blocked by a ridge in the case of SP3 (Figure A1). We assume, that this topographic barrier made up from loose, porous material causes diffraction and absorption, leading to this contrast in peak amplitude.

The jet from S1 on 15 May 2019 at 12:14 UTC was recorded successfully by four SPs. In order to calculate the propagation velocity, we measured the distance of the individual SPs to the source, and corrected this distance for their difference in elevation to obtain the line-of-sight distances. We ignored the possibility that (some) sound could be generated above the

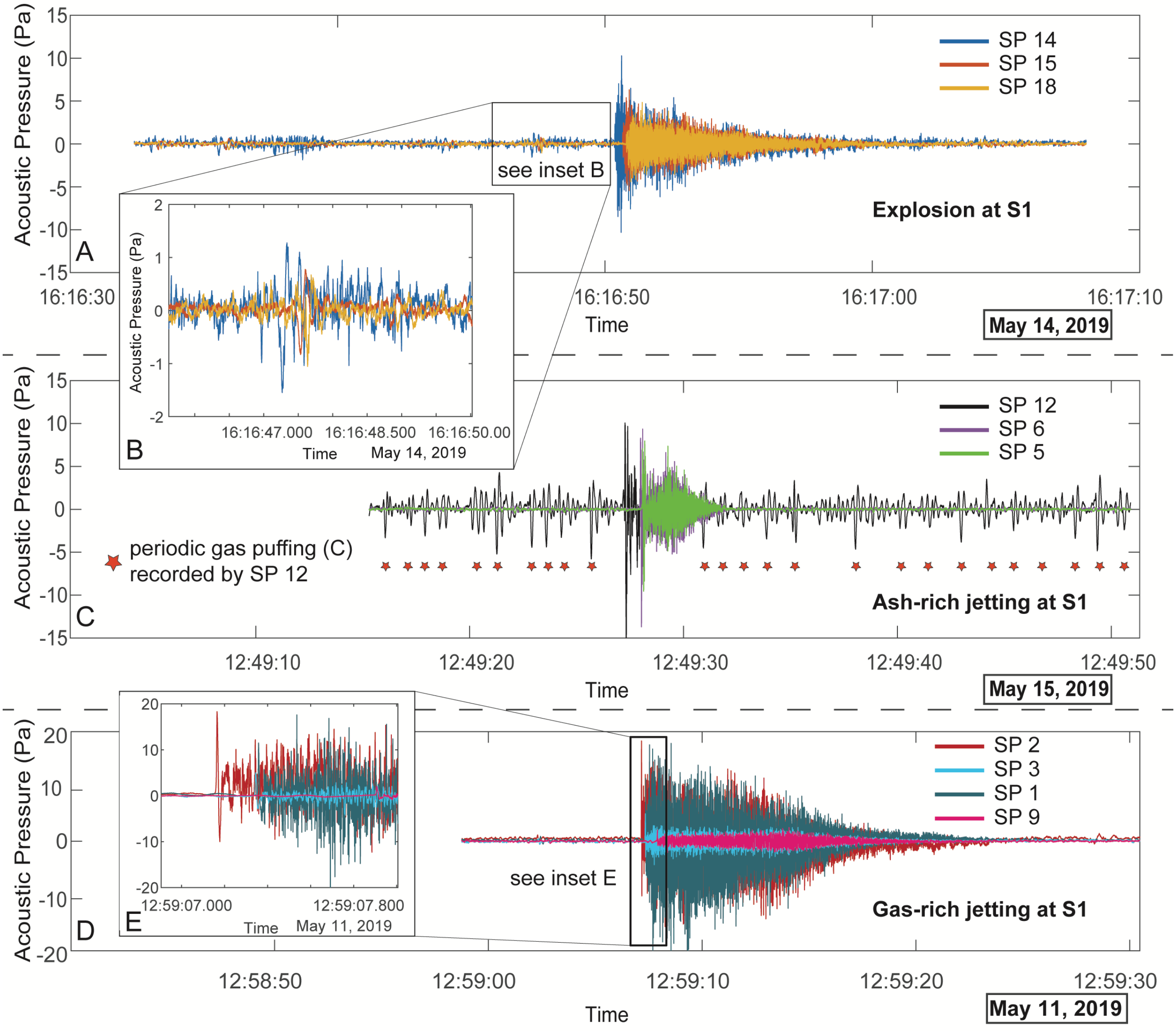

Figure 4: Three explosive events recorded at Stromboli volcano. [A] shows the acoustic signal of three SPs (#14, #15, #18) on 14 May 2019 at 16:16 UTC. Refer to Figure 3 for additional data of SP14. Smaller acoustic events before the main explosion of S1 can be seen in inset [B]. [C] On 15 May 2019 an ash-rich jet was emitted by S1 that was recorded by three SPs (#12, #6, #5). SP12 shows the acoustic signature of periodic gas puffing at the C vents. The initial waveform looks similar to the waveform of a gas-rich jetting event at S1 on 11 May 2019 [D]. Although, SP 3 and SP 4 have almost the same distance to the source of the jet their maximum pressure amplitude differs considerably (17.9 Pa, #1 and 5 Pa, #3). [E] shows the steep initial waveforms recorded by the active SPs. All SPs are listed according to their distance from the vent beginning with the closest SP.

vent [Peña Fernández et al. 2020] and assumed the vent as acoustic source. We use the temperature of 25 °C recorded by SP 12 to calculate the speed of sound to be 346.3 m s^{-1}. Based on the delay of arrival of the acoustic signal at the four SPs, different travel times can be calculated: 250 m s^{-1} to SP12, 330 m s^{-1} to SP5 and 349 m s^{-1} to SP6. As the amount of ejected ash was minor, we relate these considerably different apparent travel times to an effect of the topography, i.e. the acoustic wave propagation was strongly affected close to the surface and the assumption of linear radial expansion does not hold.

From a technical point of view, the deployment process worked well, and it became apparent that having a low-tech drop-off mechanism at each sensor is advantageous. This way, no modification of the UAV was required providing its full functionality. Although the used UAV has no nominal payload capacity, the flight characteristics and battery duration were not affected significantly. The transmission between base station and SPs via LoRa radio communication was suitable for the distances of <500 m required for this deployment scenario. If there is a direct line of sight without obstruction nearby the sensor, achieving a transmission distance of

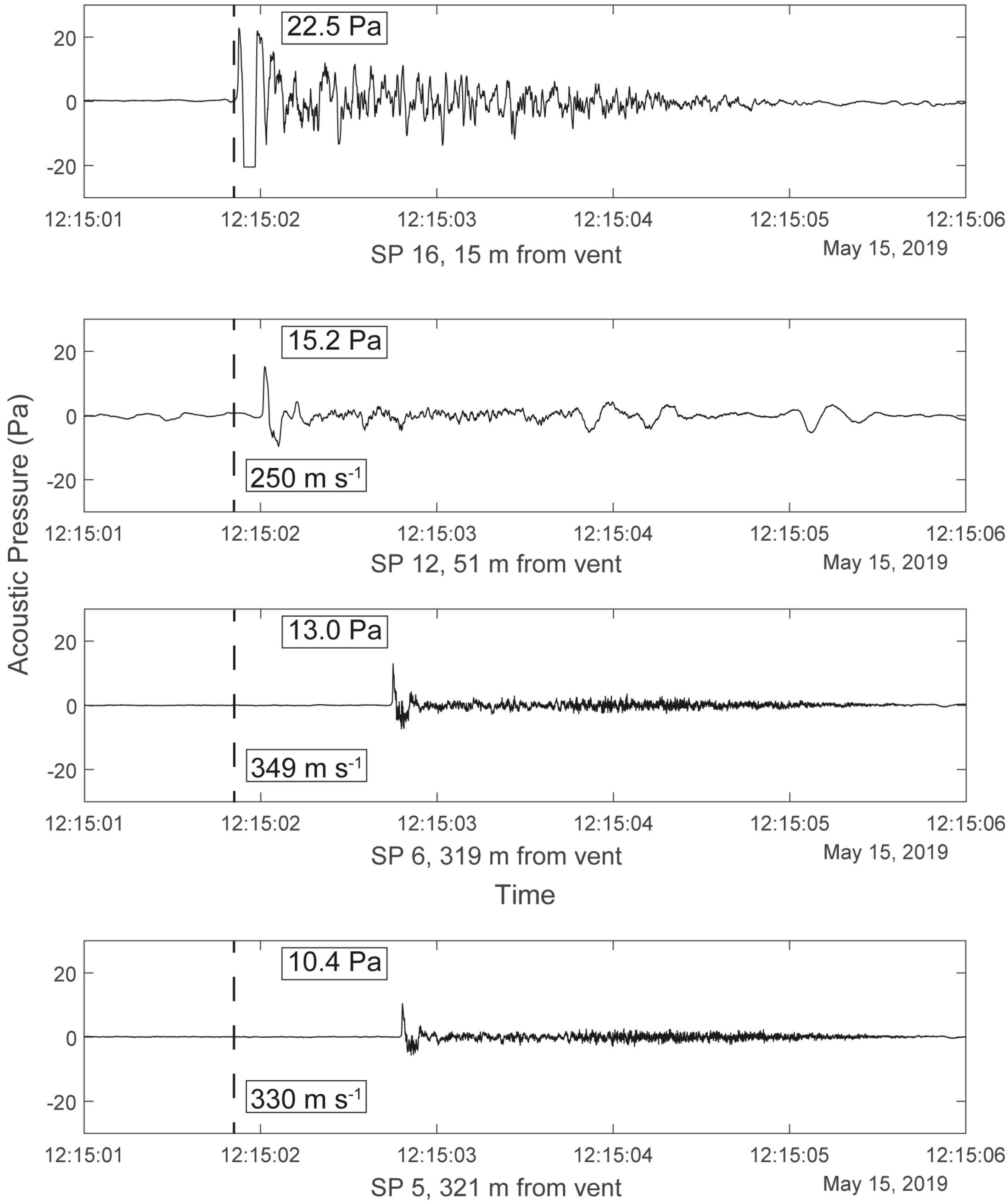

Figure 5: Acoustic pressure recorded on 15 May 2019 at 12:14 UTC by the sensors 16, 12, 5, and 6. Their vent distances range were between 15 and 321 m. The dashed line represents the onset of the acoustic event as measured by sensor 16. The boxes show the peak pressure of the first positive peak and the calculated speed of sound based on arrival times and distances between the sensors, respectively.

>2 km was possible. The biggest challenge for the radio link between SP and base station is the morphology around the sensor where the loose volcanic material can absorb a large amount of the electromagnetic wave's power.

Because the volcanic activity at Stromboli volcano was characterised by long-lasting jets during the preparation for the May 2019 campaign, the data acquisition was set up to allow for recording entire events of up to 40 s onto the ring buffer. To this end, the audio is pre-processed by making an average over 32 audio samples before the data was written to the ring buffer. This effectively filters out the acoustic signals above 500 Hz but also distorts the frequency information in the acoustic data <500 Hz. This specific type of activity was especially interesting, since it closely resembles the dynamics of shock-tube experiments [e.g. Cigala et al. 2017; Schmid et al. 2022].

We developed a novel piece of instrumentation which was successfully deployed during two field campaigns to Stromboli volcano, Italy. Through these SPs we collected near-vent data of different styles of Strombolian eruptions from multiple active vents and radio transmitted to the base station at a safe distance. While the negative correlation between the amplitude of acoustic signals and distance is known, the use of near-vent sensor platforms, as described here, shows promise for constraining proximal effects of topography and determining precisely the pressure at the vent exit.

5 Outlook

In the present study we focused on the development and the deployment of this new type of instrumentation that allows for multiparametric, in-situ measurements close to volcanic vents. We have identified shortcomings and limitations that are currently being tackled for SP generation 3.0. Amongst planned modifications are:

- to record acoustic data with lower sample rate while preserving the frequency information of the signal,
- to calibrate the microphones before and during the field deployment to ensure high-quality data,
- to improve the transmission range by using more efficient antennas,
- to develop a new sensor firmware to enable continuous real-time data streaming to a stationary base station to avoid observational bias by only triggering a specific type of event, and
- to update the housing to increase the resistivity to adverse meteorological, thermal and chemical factors.

Ultimately, this type of proximal measurement can aid vastly in constraining the pressure setting at and around volcanic vents for individual volcanic explosions. The dynamic evolution of this parameter, the duration of the eruptive event, the time delay between gas and pyroclast ejection as well as jet characteristics can be used for a quantitative description of the driving forces in the shallow plumbing system based on empirical findings from well-controlled laboratory experiments. To this end, it is desirable to deploy several SPs at different locations on or near the rim of the target vent. By deploying sensors close to the source, it is possible to measure pristine signals that are not yet affected by attenuation or pathway effects. Moreover, measuring close to the source allows detection of signals that are too weak to be measured at distances suitable for application of conventional instrumentation.

Author Contributions

U.K. and J.H. developed the idea for the first sensor generation. U.K., J.H. and M.S. field tested the first sensor generation. J.H. developed the hardware and software of all sensor generations. U.K., J.H., M.S. and D.B.D. deployed the second generation in the field. M.S. analysed the data and drafted the first manuscript. All authors discussed the data and agreed on the manuscript.

Acknowledgements

M.S. and U.K. acknowledge support through the VERTIGO Marie Curie ITN (grant agreement 607905). D.B.D. and M.S. acknowledge the support of the European Research Council Advanced Grant ERC-2018-ADG No. 834225 (EAVESDROP). The authors thank Piergiorgio Scarlato, Tullio Ricci and Jacopo Taddeucci for their logistic support during field work organisation. U.K. and M.S. thank Brett Walker, Emma Liu and Tullio Ricci for helping during drone operations and discussions. U.K. acknowledges Maurizio Ripepe and Valeria Cigala for acoustic discussions. We thank the editor Tom Pering for handling our manuscript and the two anonymous reviewers for their constructive input.

Data Availability

More information about technical details and the data can be made available upon request to the corresponding author.

Copyright notice

References

Behnke, S. A. and S. R. McNutt (2014). "Using lightning observations as a volcanic eruption monitoring tool". *Bulletin of Volcanology* 76(8). ISSN: 1432-0819. DOI: 10.1007/s00445-014-0847-1.

Bennett, A. J., P. Odams, D. Edwards, and Þ. Arason (2010). "Monitoring of lightning from the April–May 2010 Eyjafjallajökull volcanic eruption using a very low frequency lightning location network". *Environmental Research Letters* 5(4), page 044013. ISSN: 1748-9326. DOI: 10.1088/1748-9326/5/4/044013.

Caplan-Auerbach, J., A. Bellesiles, and J. K. Fernandes (2010). "Estimates of eruption velocity and plume height from infrasonic recordings of the 2006 eruption of Augustine Volcano, Alaska". *Journal of Volcanology and Geothermal Research* 189(1–2), pages 12–18. ISSN: 0377-0273. DOI: 10.1016/j.jvolgeores.2009.10.002.

Carn, S., L. Clarisse, and A. Prata (2016). "Multi-decadal satellite measurements of global volcanic degassing". *Journal of Volcanology and Geothermal Research* 311, pages 99–134. ISSN: 0377-0273. DOI: 10.1016/j.jvolgeores.2016.01.002.

Cigala, V., U. Kueppers, J. J. Peña Fernández, and D. B. Dingwell (2021). "Linking gas and particle ejection dynamics to boundary conditions in scaled shock-tube experiments". *Bulletin of Volcanology* 83(8). ISSN: 1432-0819. DOI: 10.1007/s00445-021-01473-0.

Cigala, V., U. Kueppers, J. J. Peña Fernández, J. Taddeucci, J. Sesterhenn, and D. B. Dingwell (2017). "The dynamics of volcanic jets: Temporal evolution of particles exit velocity from shock-tube experiments". *Journal of Geophysical Research: Solid Earth* 122(8), pages 6031–6045. ISSN: 2169-9313. DOI: 10.1002/2017jb014149.

Cimarelli, C. and K. Genareau (2021). "A review of volcanic electrification of the atmosphere and volcanic lightning". *Journal of Volcanology and Geothermal Research* 422, page 107449. ISSN: 0377-0273. DOI: 10.1016/j.jvolgeores.2021.107449.

Civico, R., T. Ricci, P. Scarlato, D. Andronico, M. Cantarero, B. B. Carr, E. D. Beni, E. D. Bello, J. B. Johnson, U. Kueppers, L. Pizzimenti, M. Schmid, K. Strehlow, and J. Taddeucci (2021). "Unoccupied Aircraft Systems (UASs) Reveal the Morphological Changes at Stromboli Volcano (Italy) before, between, and after the 3 July and 28 August 2019 Paroxysmal Eruptions". *Remote Sensing* 13(15), page 2870. DOI: 10.3390/rs13152870.

De Angelis, S., A. Diaz-Moreno, and L. Zuccarello (2019). "Recent Developments and Applications of Acoustic Infrasound to Monitor Volcanic Emissions". *Remote Sensing* 11(11), page 1302. ISSN: 2072-4292. DOI: 10.3390/rs11111302.

Delle Donne, D., M. Ripepe, G. Lacanna, G. Tamburello, M. Bitetto, and A. Aiuppa (2016). "Gas mass derived by infrasound and UV cameras: Implications for mass flow rate". *Journal of Volcanology and Geothermal Research* 325, pages 169–178. ISSN: 0377-0273. DOI: 10.1016/j.jvolgeores.2016.06.015.

Fee, D., P. Izbekov, K. Kim, A. Yokoo, T. Lopez, F. Prata, R. Kazahaya, H. Nakamichi, and M. Iguchi (2017). "Eruption mass estimation using infrasound waveform inversion and ash and gas measurements: Evaluation at Sakurajima Volcano, Japan". *Earth and Planetary Science Letters* 480, pages 42–52. ISSN: 0012-821X. DOI: 10.1016/j.epsl.2017.09.043.

Fee, D. and R. S. Matoza (2013). "An overview of volcano infrasound: From hawaiian to plinian, local to global". *Journal of Volcanology and Geothermal Research* 249, pages 123–139. ISSN: 0377-0273. DOI: 10.1016/j.jvolgeores.2012.09.002.

Freire, S., A. Florczyk, M. Pesaresi, and R. Sliuzas (2019). "An Improved Global Analysis of Population Distribution in Proximity to Active Volcanoes, 1975–2015". *ISPRS International Journal of Geo-Information* 8(8), page 341. ISSN: 2220-9964. DOI: 10.3390/ijgi8080341.

Garcés, M. A. (2000). "Theory of acoustic propagation in a multi-phase stratified liquid flowing within an elastic-walled conduit of varying cross-sectional area". *Journal of Volcanology and Geothermal Research* 101(1-2), pages 1–17. DOI: 10.1016/s0377-0273(00)00155-4.

Garcés, M. A., D. Fee, R. Matoza, S. A. Fagents, T. Gregg, and R. Lopes (2013). "Volcano acoustics". *Modeling volcanic processes: The physics and mathematics of volcanism*. Edited by S. A. Fagents, T. K. P. Gregg, and R. M. C. Lopes. Cambridge University Press New York, NY, pages 359–383. ISBN: 978-0-521-89543-9.

Gaudin, D. and C. Cimarelli (2019). "The electrification of volcanic jets and controlling parameters: A laboratory study". *Earth and Planetary Science Letters* 513, pages 69–80. ISSN: 0012-821X. DOI: 10.1016/j.epsl.2019.02.024.

Goto, A., M. Ripepe, and G. Lacanna (2014). "Wideband acoustic records of explosive volcanic eruptions at Stromboli: New insights on the explosive process and the acoustic source". *Geophysical Research Letters* 41(11), pages 3851–3857. ISSN: 0094-8276. DOI: 10.1002/2014gl060143.

Hargie, K. A., A. R. Van Eaton, L. G. Mastin, R. H. Holzworth, J. W. Ewert, and M. Pavolonis (2019). "Globally detected volcanic lightning and umbrella dynamics during the 2014 eruption of Kelud, Indonesia". *Journal of Volcanology and Geothermal Research* 382, pages 81–91. ISSN: 0377-0273. DOI: 10.1016/j.jvolgeores.2018.10.016.

Ishii, K., A. Yokoo, M. Iguchi, and E. Fujita (2020). "Utilizing the solution of sound diffraction by a thin screen to evaluate infrasound waves attenuated around volcano topography". *Journal of Volcanology and Geothermal Research* 402, page 106983. ISSN: 0377-0273. DOI: 10.1016/j.jvolgeores.2020.106983.

James, M., B. Carr, F. D'Arcy, A. Diefenbach, H. Dietterich, A. Fornaciai, E. Lev, E. Liu, D. Pieri, M. Rodgers, B. Smets, A. Terada, F. von Aulock, T. Walter, K. Wood, and E. Zorn (2020). "Volcanological applications of unoccupied aircraft systems (UAS): Developments, strategies, and future challenges". *Volcanica*, pages 67–114. ISSN: 2610-3540. DOI: 10.30909/vol.03.01.67114.

Johnson, J. B. (2003). "Generation and propagation of infrasonic airwaves from volcanic explosions". *Journal of Volcanology and Geothermal Research* 121(1-2), pages 1–14. DOI: 10.1016/s0377-0273(02)00408-0.

– (2004). "Volcanic eruptions observed with infrasound". *Geophysical Research Letters* 31(14). ISSN: 0094-8276. DOI: 10.1029/2004gl020020.

Johnson, J. B. and A. J. C. Miller (2014). "Application of the Monopole Source to Quantify Explosive Flux during Vulcanian Explosions at Sakurajima Volcano (Japan)". *Seismological Research Letters* 85(6), pages 1163–1176. ISSN: 1938-2057. DOI: 10.1785/0220140058.

Johnson, J. B. and M. Ripepe (2011). "Volcano infrasound: A review". *Journal of Volcanology and Geothermal Research* 206(3–4), pages 61–69. ISSN: 0377-0273. DOI: 10.1016/j.jvolgeores.2011.06.006.

Johnson, J. B., M. C. Ruiz, H. D. Ortiz, L. M. Watson, G. Viracucha, P. Ramon, and M. Almeida (2018). "Infrasound Tornillos Produced by Volcán Cotopaxi's Deep Crater". *Geophysical Research Letters* 45(11), pages 5436–5444. ISSN: 1944-8007. DOI: 10.1029/2018gl077766.

Kim, K., D. Fee, A. Yokoo, and J. M. Lees (2015). "Acoustic source inversion to estimate volume flux from volcanic explosions". *Geophysical Research Letters* 42(13), pages 5243–5249. ISSN: 0094-8276. DOI: 10.1002/2015gl064466.

Kobayashi, T., A. Namiki, and I. Sumita (2010). "Excitation of airwaves caused by bubble bursting in a cylindrical conduit: Experiments and a model". *Journal of Geophysical Research* 115(B10). ISSN: 0148-0227. DOI: 10.1029/2009jb006828.

Koyaguchi, T., Y. J. Suzuki, and T. Kozono (2010). "Effects of the crater on eruption column dynamics". *Journal of Geophysical Research* 115(B7). ISSN: 0148-0227. DOI: 10.1029/2009jb007146.

Lacanna, G. and M. Ripepe (2013). "Influence of near-source volcano topography on the acoustic wavefield and implication for source modeling". *Journal of Volcanology and Geothermal Research* 250, pages 9–18. ISSN: 0377-0273. DOI: 10.1016/j.jvolgeores.2012.10.005.

– (2020). "Modeling the Acoustic Flux Inside the Magmatic Conduit by 3D-FDTD Simulation". *Journal of Geophysical Research: Solid Earth* 125(6). ISSN: 2169-9356. DOI: 10.1029/2019jb018849.

Lamb, O. D., S. De Angelis, and Y. Lavallée (2015). "Using infrasound to constrain ash plume rise". *Journal of Applied Volcanology* 4(1). ISSN: 2191-5040. DOI: 10.1186/s13617-015-0038-6.

Lorenz, R. D., E. P. Turtle, R. Howell, J. Radebaugh, and R. M. Lopes (2016). "The roar of Yasur: Handheld audio recorder monitoring of Vanuatu volcanic vent activity". *Journal of Volcanology and Geothermal Research* 322, pages 168–174. DOI: 10.1016/j.jvolgeores.2015.06.019.

Maher, S. P., R. S. Matoza, C. D. Groot-Hedlin, K. L. Gee, D. Fee, and A. Yokoo (2020). "Investigating Spectral Distortion of Local Volcano Infrasound by Nonlinear Propagation at Sakurajima Volcano, Japan". *Journal of Geophysical Research: Solid Earth* 125(3). ISSN: 2169-9356. DOI: 10.1029/2019jb018284.

Matoza, R. S., D. Fee, D. Green, and P. Mialle (2019). "Volcano Infrasound and the International Monitoring System". *Infrasound Monitoring for Atmospheric Studies*. Springer International Publishing, pages 1023–1077. DOI: 10.1007/978-3-319-75140-5_33.

Matoza, R. S., D. Fee, T. B. Neilsen, K. L. Gee, and D. E. Ogden (2013). "Aeroacoustics of volcanic jets: Acoustic power estimation and jet velocity dependence". *Journal of Geophysical Research: Solid Earth* 118(12), pages 6269–6284. ISSN: 2169-9313. DOI: 10.1002/2013jb010303.

McKee, K., D. Fee, A. Yokoo, R. S. Matoza, and K. Kim (2017). "Analysis of gas jetting and fumarole acoustics at Aso Volcano, Japan". *Journal of Volcanology and Geothermal Research* 340, pages 16–29. ISSN: 0377-0273. DOI: 10.1016/j.jvolgeores.2017.03.029.

McNutt, S. R. and E. R. Williams (2010). "Volcanic lightning: global observations and constraints on source mechanisms". *Bulletin of Volcanology* 72(10), pages 1153–1167. ISSN: 1432-0819. DOI: 10.1007/s00445-010-0393-4.

Muramatsu, D., K. Aizawa, A. Yokoo, M. Iguchi, and T. Tameguri (2018). "Estimation of Vent Radii From Video Recordings and Infrasound Data Analysis: Implications for Vulcanian Eruptions From Sakurajima Volcano, Japan". *Geophysical Research Letters* 45(23). ISSN: 1944-8007. DOI: 10.1029/2018gl079898.

Ogden, D. E., K. H. Wohletz, G. A. Glatzmaier, and E. E. Brodsky (2008). "Numerical simulations of volcanic jets: Importance of vent overpressure". *Journal of Geophysical Research* 113(B2). ISSN: 0148-0227. DOI: 10.1029/2007jb005133.

Peña Fernández, J. J., V. Cigala, U. Kueppers, and J. Sesterhenn (2020). "Acoustic analysis of starting jets in an anechoic chamber: implications for volcano monitoring". *Scientific Reports* 10(1). DOI: 10.1038/s41598-020-69949-1.

Pering, T. D., E. J. Liu, K. Wood, T. C. Wilkes, A. Aiuppa, G. Tamburello, M. Bitetto, T. Richardson, and A. J. S. McGonigle (2020). "Combined ground and aerial measurements resolve vent-specific gas fluxes from a multi-vent volcano". *Nature Communications* 11(1). DOI: 10.1038/s41467-020-16862-w.

Rakov, V. A. (2013). "Electromagnetic Methods of Lightning Detection". *Surveys in Geophysics* 34(6), pages 731–753. ISSN: 1573-0956. DOI: 10.1007/s10712-013-9251-1.

Ripepe, M., C. Bonadonna, A. Folch, D. Delle Donne, G. Lacanna, E. Marchetti, and A. Höskuldsson (2013). "Ash-plume dynamics and eruption source parameters by infrasound and thermal imagery: The 2010 Eyjafjallajökull eruption". *Earth and Planetary Science Letters* 366, pages 112–121. ISSN: 0012-821X. DOI: 10.1016/j.epsl.2013.02.005.

Ripepe, M., S. Ciliberto, and M. Della Schiava (2001). "Time constraints for modeling source dynamics of volcanic explosions at Stromboli". *Journal of Geophysical Research: Solid Earth* 106(B5), pages 8713–8727. ISSN: 0148-0227. DOI: 10.1029/2000jb900374.

Ripepe, M. and E. Marchetti (2002). "Array tracking of infrasonic sources at Stromboli volcano". *Geophysical Research Letters* 29(22), pages 33-1–33–4. ISSN: 0094-8276. DOI: 10.1029/2002gl015452.

Schmid, M., U. Kueppers, V. Cigala, and D. B. Dingwell (2022). "Complex geometry of volcanic vents and asymmetric particle ejection: experimental insights". *Bulletin of Volcanology* 84(8). ISSN: 1432-0819. DOI: 10.1007/s00445-022-01580-6.

Schmid, M., U. Kueppers, V. Cigala, J. Sesterhenn, and D. B. Dingwell (2020). "Release characteristics of overpressurised gas from complex vents: implications for volcanic hazards". *Bulletin of Volcanology* 82(11). ISSN: 1432-0819. DOI: 10.1007/s00445-020-01407-2.

Schmid, M., U. Kueppers, R. Civico, T. Ricci, J. Taddeucci, and D. B. Dingwell (2021). "Characterising vent and crater shape changes at Stromboli: implications for risk areas". *Volcanica* 4(1), pages 87–105. ISSN: 2610-3540. DOI: 10.30909/vol.04.01.87105.

Taddeucci, J., J. J. Peña Fernández, V. Cigala, U. Kueppers, P. Scarlato, E. Del Bello, T. Ricci, J. Sesterhenn, and S. Panunzi (2021). "Volcanic Vortex Rings: Axial Dynamics, Acoustic Features, and Their Link to Vent Diameter and Supersonic Jet Flow". *Geophysical Research Letters* 48(15). ISSN: 1944-8007. DOI: 10.1029/2021gl092899.

Taddeucci, J., J. Sesterhenn, P. Scarlato, K. Stampka, E. D. Bello, J. J. Peña Fernández, and D. Gaudin (2014). "High-speed imaging, acoustic features, and aeroacoustic computations of jet noise from Strombolian (and Vulcanian) explosions". *Geophysical Research Letters* 41(9), pages 3096–3102. DOI: 10.1002/2014gl059925.

Tam, C. K. W. (1995). "Supersonic Jet Noise". *Annual Review of Fluid Mechanics* 27(1), pages 17–43. DOI: 10.1146/annurev.fl.27.010195.000313.

Vergniolle, S., G. Brandeis, and J.-C. Mareschal (1996). "Strombolian explosions: 2. Eruption dynamics determined from acoustic measurements". *Journal of Geophysical Research: Solid Earth* 101(B9), pages 20449–20466. ISSN: 0148-0227. DOI: 10.1029/96jb01925.

Vidal, V., M. Ripepe, T. Divoux, D. Legrand, J.-C. Géminard, and F. Melo (2010). "Dynamics of soap bubble bursting and its implications to volcano acoustics". *Geophysical Research Letters* 37(7), n/a–n/a. ISSN: 0094-8276. DOI: 10.1029/2009gl042360.

Vossen, C. E. J., C. Cimarelli, A. J. Bennett, A. Geisler, D. Gaudin, D. Miki, M. Iguchi, and D. B. Dingwell (2021). "Long-term observation of electrical discharges during persistent Vulcanian activity". *Earth and Planetary Science Letters* 570, page 117084. ISSN: 0012-821X. DOI: 10.1016/j.epsl.2021.117084.

Vossen, C. E. J., C. Cimarelli, A. J. Bennett, M. Schmid, U. Kueppers, T. Ricci, and J. Taddeucci (2022). "The electrical signature of mafic explosive eruptions at Stromboli volcano, Italy". *Scientific Reports* 12(1). ISSN: 2045-2322. DOI: 10.1038/s41598-022-12906-x.

Watson, L. M., E. M. Dunham, and J. B. Johnson (2019). "Simulation and inversion of harmonic infrasound from open-vent volcanoes using an efficient quasi-1D crater model". *Journal of Volcanology and Geothermal Research* 380, pages 64–79. ISSN: 0377-0273. DOI: 10.1016/j.jvolgeores.2019.05.007.

Woulff, G. and T. R. McGetchin (1976). "Acoustic Noise from Volcanoes: Theory and Experiment". *Geophysical Journal International* 45(3), pages 601–616. ISSN: 1365-246X. DOI: 10.1111/j.1365-246x.1976.tb06913.x.

Appendix A

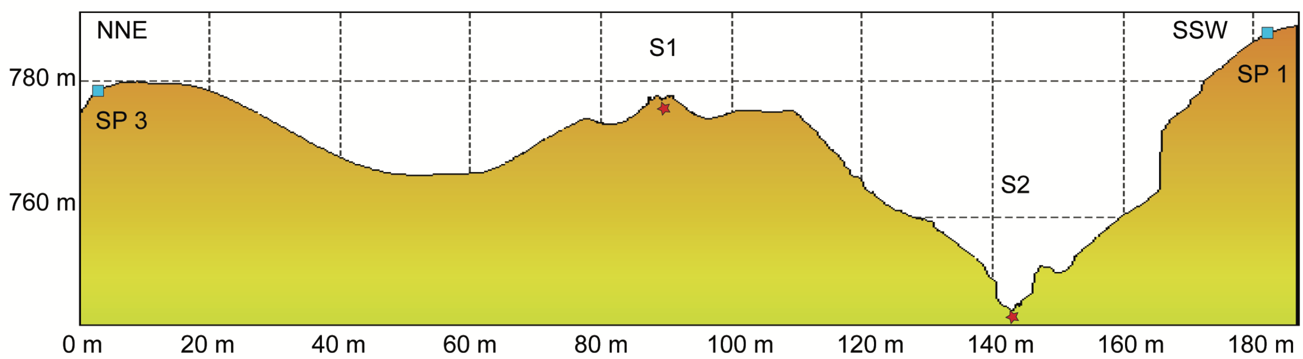

Figure A1: Transect through the crater terrace of Stromboli volcano, Italy. The transect starts in the NNE, close to the location of SP3, and continues through vent S1 and S2 towards the SSW close to the location of SP1 (Figure 2). The transect was created from a digital elevation model (DEM) of the crater terrace at the time of the field campaign. Refer to Schmid et al. [2021] for a description of the DEM processing.